PHOTODISSOCIATION OF PERNITRIC ACID (HO_2NO_2) AT 248 nm*

Hélene MacLeod,† Gregory P. Smith, and David M. Golden
Department of Chemical Kinetics
Chemical Physics Laboratory
SRI International, Menlo Park, CA 94025

ABSTRACT

The photodissociation of pernitric acid (PNA) has been studied at 248 nm. The quantum yield for production of OH radicals is 34 ± 16%. The yield of OH from PNA was measured relative to that from H_2O_2. The translational and rotational energy content of the OH photofragment from PNA has been characterized. A fluorescent emission was also observed and characterized. It is attributed to electronically excited NO_2 produced in the PNA photodissociation. A maximum yield of 30% for NO_2^* production was determined. The intensity of this emission, and a mass spectrometric peak at m/e = 33, have been found to be useful means of characterizing the purity of the PNA sample.

*This work was supported by Contract No. NAS 3888 with the National Aeronautics and Space Administration.

†Postdoctoral Research Associate. Present address: CRCCHT, CNRS, 1C av. de la Recherche Scientifique, 45045-Orleans, Cedex, France.

CK 87-17
Submitted to J. Chem. Phys., 5/21/87

I INTRODUCTION

Peroxynitric acid (PNA), HO_2NO_2, is formed in the atmosphere by combination of the HO_2 radical with NO_2.[1] Its reaction with OH radicals is a key to the catalytic cycles involving odd-hydrogen radicals (HO_x) in the lower stratosphere and has been the subject of several experimental investigations.[2,3,4] To fully characterize the chemistry of PNA under atmospheric conditions its photolytic rate and products must be specified. Currently the only experimental information with respect to the photochemistry is the photoabsorption cross section of PNA.[5] A recent theoretical study[6] has identified the low-lying excited states of this molecule and their likely dissociation products. In this article we report a first experimental study of photolytic pathways in PNA.

The photoabsorption cross section of PNA falls rapidly from 10^{-17} cm^2 at 190 nm to 10^{-21} cm^2 at 330 nm.[5] This trend is consistent with the theoretical work[6] which places the lowest excited state of PNA near 5 eV. This electronic state is expected to lead to the dissociation of PNA. Altogether eight dissociative channels are energetically accessible from this state. We chose to perform this first photolysis study at 248 nm, where the absorption cross section is large. The data obtained are likely to be applicable to the atmospherically important 290 nm range since in both cases the same electronic state in PNA is accessed and the same product channels are open. Our reasoning for performing the first study at 248 nm is due to the fact that the cross section at this wavelength is twenty times larger than at 290 nm.

Two of the photodissociation pathways were characterized quantitatively and found to be important. These are:

$$HO_2NO_2 + h\nu \rightarrow OH + \text{products}$$

and

$$HO_2NO_2 + h\nu \rightarrow NO_2^* + HO_2$$

The quantum yield for the first channel is roughly one third, while that for the second is less than 30%. The remaining majority photoproducts are most likely ground state $NO_2 + HO_2$.

II EXPERIMENTAL

All experiments were performed in a very low pressure photolysis reactor (VLPΦ). The reactant gas is monitored by mass spectrometry. Photolysis is produced by a 248 nm excimer laser. OH photofragments are monitored by laser induced fluorescence (LIF). Their concentration is calibrated relative to those produced in photodissociation of H_2O_2. The fluorescence emission from PNA is analyzed with a grating monochromator. In the following section, we discuss the experimental methods used in some detail.

Very Low-Pressure Photolysis Cell (VLPΦ)

The experimental apparatus, shown in Figure 1, consists of a VLPΦ reactor mounted on a modulated molecular beam mass spectrometer, and has been described in detail previously.[7] The reactor is a T-shaped pyrex cell coated

with halocarbon wax to reduce the wall decomposition of PNA and H_2O_2. The gases flow into the reactor from the preparation line (described below) and escape from the reactor into a vacuum through a small aperture (~1 mm diameter). The effusive molecular beam thus formed is modulated by a tuning-fork chopper (200 Hz), analyzed by an electron impact quadrupole mass spectrometer (Balzers QMG 311), and detected using a lock-in amplifier. The vacuum system consists of two differentially pumped chambers. The first chamber is pumped by a 270 l/s turbo-molecular pump to a residual pressure of ~8 x 10^{-7} Torr. The second chamber which contains the quadrupole mass filter is pumped by a 110 l/s turbo-molecular pump to a residual pressure of ~8 x 10^{-8} Torr. These pumping speeds create a residual pressure of ~5 x 10^{-5} Torr in the VLPΦ cell.

The cell is a 35-cm long, 2.5-cm diameter tube crossed by a second 10-cm long tube (see Figure 1). All tube ends feature O-ring sealed quartz windows or glued windows at Brewster's angle. A fifth window is located perpendicular to the intersecting tube sections for the detection of the laser-induced fluorescence (LIF) light. The cell volume is ~330 cm^3; the residence time in the cell is ~4.6 s for PNA and ~3 s for H_2O_2. The pressure is monitored by a capacitance manometer.

The photolysis laser is a Lumonics TE-860-3 excimer laser, operating at 10 Hz on the KrF line at 248 nm, with a typical pulse energy of 20 mJ/cm^2. The excimer beam is mildly focused and is guided through four 1.5 cm diameter apertures that define the beam path and the beam size. The beam fills 20% of the entire cell volume.

Laser-Induced Fluorescence (LIF) Detection of OH Radicals. A Lambda Physik excimer-pumped dye laser (EMG 101-FL2002), frequency doubled, operated at 10 Hz, 15 μJ/pulse, is tuned between 281 and 284 nm to excite one of the rotational transitions of the OH(A-X) (1,0) band. The dye-laser beam (0.5-cm diameter) is directed at right angles to the photolysis laser beam through the shorter tube. Fluorescence in the A-X (1,1) band of OH is detected by imaging the intersection of the laser beams onto a filtered 1P28A photomultiplier tube (PMT). A narrow-band interference filter centered at 313 nm ± 10 nm and a long-pass cutoff filter to discriminate against scattered photolysis laser light were used. Signals are amplified, (10 times, 50 ohm impedence) and processed by a boxcar integrator (PAR 164). A delay generator provides a variable delay time (Δt) between the excimer pulse and the dye pulse.

Detection of the PNA Fluorescence Emission. An intense fluorescence emission from PNA was also detected by the filtered PMT upon irradiation by the photolysis laser alone. The window used for the dye-laser beam input in the LIF experiment (Figure 1) was used alternatively to monitor this PNA fluorescence emission. The fluorescence light was collected with an f/1 lens, collimated with an f/2 lens and focused on the entrance slit of a 0.46-m monochromator (MPI model 1018A), which has a grating blazed at 6000 Å. The resolution was typically 5 nm with a slit width of 3 mm. The fluorescence was detected at the exit of the monochromator by either a Hammamatsu R666 PMT or an RCA 1P28 PMT. The R666 PMT has a flat response curve between 300 and 800 nm, while the 1P28 PMT response is maximum at 320 nm and falls off rapidly in the visible (50% of maximum at 500 nm). The RCA 1P28 PMT has a higher maximum sensitivity by two orders of magnitude than the R666 PMT. Therefore, we

mainly used the 1P28 PMT, although it is less sensitive in the red than the R666 PMT. The signal from the PMT is amplified (10 times) and processed by a boxcar averager (SRS model SR250). A long pass cutoff filter (Schott glass WG305) is placed in front of the entrance slit of the monochromator to eliminate the scattered excimer light. In addition, the lifetime of the fluorescence emission was monitored with a transient digitizer (Transiac 2001).

Pernitric Acid Preparation and Detection. Pernitric acid (HO_2NO_2) is both a strong acid and a peroxynitrate. This very unstable compound decomposes on many surfaces such as pyrex, and metals.[3] We synthesized it in small batches, in a nitrogen atmosphere glove box, by adding 1.2 g of solid NO_2BF_4 (Sharpe Chemicals) to a 4-g solution of 90% H_2O_2 (FMC) in a 50 cm^3 vessel kept at 0°C.[8] The vessel is connected to the preparation line, and immediately after the reaction is completed it is pumped down at 0°C. The preparation line includes a U-trap kept at -15°C to trap H_2O_2 vapors and a needle valve to regulate the PNA flow into the reactor. All parts of the preprartion line are made of either Teflon or pyrex coated with halocarbon wax in order to reduce wall decomposition of PNA and H_2O_2.

The PNA synthesis decsribed above is known[5] to produce the following impurities: H_2O_2 (~25%), HNO_3 (~10%), NO_2 (~5%), and SiF_4 (<5%). The concentrations of PNA and these impurities are monitored by mass spectrometry. The mass spectra cannot provide an absolute unambiguous measurement of the PNA concentration due to the fact that HNO_3, NO_2 and PNA all possess identical main peaks at m/e = 30 and 46. Calibration of the mass spectrometer for pure HNO_3 appears somewhat irreproducible (probably because it absorbs on

the ion source), and cannot be done repeatedly because HNO_3 tends to destroy the effectiveness of the wall coating. The mass spectrometer can, however, be used to determine the approximate level of impurities, which varies from batch to batch, and the level of wall decomposition, which can vary during a given run and differ from run to run. Wall decomposition of PNA mainly produces H_2O, O_2, and NO_2. It is kept to a minimum by maintaining a clean, frequently recoated system, by flowing the PNA solution from a constant temperature bath (0 to 2°C). At this temperature, the vapor pressure above the PNA solution is 2 to 5 Torr and steady concentrations between 10 and 200 mTorr can be obtained in the VLPΦ cell during a few hours for one batch of PNA. Figure 2 shows a typical spectrum of PNA effusing from the reactor. The resolution was one mass unit at mass 63. In Table 1, we give the mass spectrometric sensitivities of PNA and those of pure samples of HNO_3, NO_2, and H_2O_2 used for calibration of the mass spectrometer. As mentioned above, the values for HNO_3 are approximate, especially for the small parent peak at m/e = 63. The series of very small peaks (m/e = 62, 66, 73, 77, 81) is attributed to small levels of impurities, such as SiF_4, and products of PNA reactions with the wall coating.

III RESULTS

The results of our study of PNA photolysis at 248 nm can be subdivided into three areas. One is the characterization of the fluorescence emission observed upon photodissociation of PNA. The second is the determination of the quantum yield for production of OH radicals by photodissociation of PNA at 248 nm. The third area is the information obtained from the mass spectrometry

data recorded simultaneously with the OH quantum yield measurements. The OH quantum yield measurements were conducted at low PNA pressure (4-40 mTorr). The mass spectrometer was usually not operated during the study of the fluorescence emission because these experiments required higher PNA pressure (100-200 mTorr) in the reactor in order to obtain enough dispersed fluorescence signal.

A. Fluorescence Emission

A typical wavelength spectrum recorded for the dispersed fluorescence emission following excitation of PNA by the excimer laser is shown in Figure 3. This spectrum was recorded using the R666 PMT at a 50 ns delay time after the excimer laser pulse and with a 1 μs observation gate. The dominant feature of the fluorescence spectrum is a broadband emission with an onset near 400 nm and a maximum around 558 nm. A small additional feature in the spectrum is an emission from electronically excited OH at 309 nm (1st order) and 618 nm (2nd order). A spectrum recorded at higher resolution (Figure 3 insert) shows the structure of the R and Q branch heads of the A-X (0,0) transition of OH.[9] The R branch appears attenuated because of the presence of the long-pass cutoff filter. (It was the observation of the OH^* emission using the PMT filtered at 313 + 10 nm that led to this study of the PNA fluorescence emission).

We also observed that emission features similar to those appearing in PNA are produced by photodissociation of HNO_3 and by photoexcitation of NO_2 at 248 nm. HNO_3 and NO_2 are present as impurities from the PNA synthesis, and we therefore examined their fluorescence intensities. We observed that the emissions from pure NO_2 and HNO_3, at comparable pressures, are of much lower intensity, ruling out the possibility that the emission observed in the PNA

irradiation is produced by one of these impurities. The emission spectra that we recorded for HNO_3 and NO_2 are compared in Figure 4 with the one from PNA. The spectra shown in Figure 4 are recorded with the 1P28 phototube at a delay time of 500 ns after the excimer laser pulse and with a 1 μs observation gate. At short wavelengths, the emission from PNA has a wavelength distribution similar to the one from NO_2. Both spectra exhibit a shoulder at 460-470 nm and a short wavelength threshold near 420 nm. At long wavelengths, the emission from PNA has a wavelength distribution similar to the one from HNO_3 at long wavelengths. In the latter, the maximum is shifted towards the red (580 nm) compared to that of PNA (558 nm). The fluorescence spectrum from HNO_3 also contains an emission from electronically excited OH similar to that observed in the PNA spectra. For the three compounds, we found the intensity of the emission to vary linearly with the pressure. In Table 2, we show the measured relative fluorescence intensities of PNA, HNO_3, and NO_2 at 558 nm and the absorption cross sections of the three compounds at 248 nm.[10] The relationship between the two will be interpreted in the discussion section. The fluorescence emissions from NO_2 and HNO_3 are ~18 times and ~5 times, respectively, less intense than that from PNA at 558 nm.

To characterize the excitation mechanism that produces the fluorescence emission, we studied the laser power dependence of the fluorescence emission from PNA. This was done by monitoring the dispersed fluorescence at its maximum intensity, 558 nm, and attenuating the excimer beam with a series of quartz plates. We found the emission to be linearly dependent on laser fluence (5 to 20 mJ/pulse/cm^2), suggesting that the emitter is produced following single photon absorption of PNA. A similar study of the OH^* fluorescence intensity, monitored by the filtered PMT, showed a cubic

dependence on the photon flux. The energetics of both processes will be discussed later.

A comparison of our emission spectra from PNA, HNO_3, and NO_2, with literature spectra from NO_2 photoexcited in the visible[11,12] reveals that the emitter for all three species is likely to be NO_2^*, with different state distributions. In particular, the PNA emission spectrum that we observe is very similar to the one recently reported by Oh et. al.,[12] obtained from the photolysis of N_2O_5 at 266 nm and 304 nm, and assigned to NO_2^*. Their spectra were recorded with a PMT having a similar response curve to our R666 PMT, and they are compared to our PNA emission spectrum in Figure 3. The PNA spectrum is shifted towards the blue indicating a higher energy distribution in the excited state of NO_2. Since the dissociation energies of N_2O_5 and PNA to form $NO_2 + NO_3$ and $NO_2 + HO_2$, respectively, are very similar (7468 versus 8065 cm^{-1}), the higher energy distribution of NO_2^* from PNA is consistent with the fact that our 248 nm photolysis radiation has a higher energy.

Finally, we measured the lifetime of the NO_2^* emission from PNA in pure PNA and in the presence of argon. We monitored the emission decay at 558 nm using a transient digitizer (Transiac 2001). The lifetimes were measured as a function of PNA pressure and as a function of argon pressure. Plots of the decay rate versus pressure are shown in Figure 5. The rate constant for quenching of this emission by PNA, from the slope of the weighted linear least squares fit, is $(1.7 \pm 0.3) \times 10^{-10}$ cm^3 s^{-1}. This value is comparable to the value obtained by Donnelly, et. al.: $(1.13 \pm 0.04) \times 10^{-10}$ cm^3 s^{-1} for quenching of $NO_2(^2B_2)$, formed by visible excitation of NO_2, by NO_2 itself.[13] For the quenching of true PNA emission by argon, we found a rate constant of (2.4 ± 0.4) 10^{-11} cm^3 s^{-1}. This value is also comparable to the one measured

by Donnelly, et. al. for quenching of $NO_2(^2B_2)$ by argon: (3.9 + 0.15) 1-^{-11} cm^3 s^{-1}. (Differences may be attributed to differing excited state distributions.)

The lifetime of the OH^* emission, following photolysis of PNA at 248 nm, was observed to be shorter than 1 μs for all pressures of PNA and argon studied but was not measured in detail. This rapid decay is consistent with the known zero-pressure lifetime of $OH(A^2\Sigma^+)$ of 690 ns.[14]

B. Measurement of the OH Quantum Yield

The OH quantum yield from photodissociation of PNA was determined relative to the OH quantum yield from photodissociation of H_2O_2. The OH quantum yield from photodissociation of H_2O_2 at 248 nm is 2.[10] The OH concentration is monitored in both cases by LIF.

This calibration against the OH LIF signal from H_2O_2 is valid only if OH from H_2O_2 and OH from PNA have a similar energetic distributions at the time of detection. At 248 nm there is not enough energy to produce $OH(A^2\Sigma^+)$ in a one-photon process either from H_2O_2 or from PNA. Any dominant channel producing OH from PNA will form OH in its ground electronic state, as is known to occur for H_2O_2.[15] We now examine successively the energy distribution among vibrational, rotational and translational energy of the OH fragment from both parent molecules.

Vibrational Distribution of the OH Fragment. It is known that photodissociation of H_2O_2 at 248 nm at low pressure (~100 mTorr) produces vibrationally cold OH.[16] Although similar information is not available for PNA, it is very likely that the OH is formed mostly in v = 0. The related HONO and HNO_3

photodissociations produce OH that is vibrationally cold and translationally hot.[17,18] We note in the following section that the PNA also produces fast OH, and thus we expect similar behavior on a repulsive upper-state surface. According to a simple impulse model picture,[17,18] most excess energy should appear as translation. Because the bond length and strength for O-H in PNA and OH are nearly the same, the OH product can be expected to retain its lack of vibrational excitation.

Rotational Distribution of the OH Fragment. The photodissociation of H_2O_2 at 248 nm and at low pressure (~200 mTorr) produces OH with a high rotational temperature.[16] We conducted a series of experiments to assess the rotational distribution of the OH produced from H_2O_2 and from the PNA under our experimental conditions, as well as to determine the rate of OH rotational thermalization. To obtain the rotational distributions of OH radicals, the dye laser wavelength was scanned to obtain excitation spectra of part of the OH(A-X)(1,0) band, at different delay times following photolysis. In Figure 6, we show typical excitation spectra, one from PNA and one from H_2O_2 photodissociation, taken at a delay time of 5 μs at 20 mTorr pressure. Spectra were also recorded at delay times between 1 and 500 μs for H_2O_2 and between 2 and 10 μs for PNA. At a delay time shorter than 2 μs the excimer-laser-induced emission from PNA, described above, is too intense and overwhelms the OH LIF signal. At delay times longer than 10 μs, the OH concentration from PNA (~3 times smaller than that from H_2O_2) becomes too low to obtain reliable OH excitation spectra. The LIF intensities were converted into rotational populations using the known rotational line strengths,[19] and rotational temperatures were deduced from the least-squares fit of the data to

a Boltzmann distribution. For H_2O_2 at pressures of ~20 mTorr, the rotational temperature of OH was found to decrease from ~1200 K at 1 μs delay to ~500 K at 5 μs. For PNA at pressures between 20 and 40 mTorr, the rotational temperature of OH was found to be between 500 K and 600K at delay times between 2 and 5 μs. This indicates clearly that either OH is rotationally thermalized faster by PNA than by H_2O_2 or that OH is formed with less rotational energy in the photodissociation of PNA. We note that both HONO and HNO_3 produce rotationally cold OH photoproduct.[17,18]

Translational Energy of the OH Fragment. OH radicals are produced with very high (64 kcal/mole) translational energy in the photodissociation of H_2O_2 at 248 nm.[20] In our VLPΦ system this is illustrated by the observation that OH radicals rapidly escape from the LIF viewing region. The OH concentration as a function of time after photolysis shows an initial rapid decay (τ ~4μs) associated with this translational effect, followed by a slower decay (τ ~1 ms) due to the reaction of OH on walls or in the gas phase. We observed similar time constants for H_2O_2 at pressures of ~20 mTorr and for PNA at pressures between 20 and 40 mTorr. This indicates that OH is also produced with high kinetic energy in the photodissociation of PNA, leading therefore to comparable observation times in the LIF viewing region for the OH fragment from both H_2O_2 and PNA. On the basis of the above results, we conducted the measurements of the OH quantum yield at $\Delta t = 3$ μs, where we postulated that the rotational distributions of OH produced by PNA and H_2O_2 would be similar. At this delay time, the OH signal from PNA is high enough to be monitored accurately.

Given the supposition that at delay times of 3 μs and at pressures between 20 and 40 mTorr the rotational distribution of OH is similar in H_2O_2 and in PNA, the intensity of a single OH rotational line is proportional to the total OH concentration. We chose to monitor two different lines, the $Q_1$1,1′ and the $Q_1$5 of the OH(A-X)(1,0) band. The $Q_1$1,1′ was chosen because it is the most intense of the low rotational levels. The $Q_1$5 line was chosen because it has a higher rotational energy and is not overlapped by any other line at our laser resolution (see Figure 6).

The quantum yield measurements were then conducted as follows: Assuming that the VLPΦ cell contains pure PNA, the quantum yield for OH production from PNA, Φ, can be related to that from pure H_2O_2 through equation (1):

$$\Phi = I_{PNA}\, 2\phi_{H_2O_2} / I_{H_2O_2}\, \phi PNA \quad . \qquad (1)$$

$I_{PNA}(H_2O_2)$ is the LIF intensity of the OH line monitored, normalized to the PNA (H_2O_2) pressure, and ϕPNA (H_2O_2) is the percentage of PNA (H_2O_2) photodissociated per excimer pulse, in the volume irradiated by the laser beam:

$$\phi = (1 - e^{-\sigma n}) \quad . \qquad (2)$$

σPNA (H_2O_2) is the absorption cross section[10] of PNA (H_2O_2) at 248 nm, $\sigma_{H_2O_2} = 8.3 \times 10^{-20}$ cm^2 and σPNA $= 4.2 \times 10^{-19}$ cm^2, and n is the flux of photons per cm^2 per pulse. (The 2 in the denominator of equation (1) accounts for the fact that H_2O_2 produces two OH radicals upon photolysis while PNA can form only one OH.)

We conducted several PNA runs and several H_2O_2 runs and excited both the $Q_1 1,1'$ and the $Q_1 5$ lines. The measured intensities of the two OH LIF signals are plotted against the pressure of PNA and H_2O_2 in Figures 7 and 8. The horizontal line drawn in each figure represents the average intensity for each OH transition. The variation of the $Q_1 1,1'$ line with H_2O_2 pressure will be discussed later. The resulting normalized intensities, I_{PNA} and $I_{H_2O_2}$ are given in Table 3 together with the quantum yield ϕ calculated according to Equation (1).

All measurements were conducted at a delay time of 3 μsec and with identical conditions of signal amplification and averaging. During the H_2O_2 runs the H_2O_2 pressure was varied between 7 and 20 mTorr. During PNA runs the pressure in the reactor was varied between 5 and 35 mTorr. At the delay time the excimer laser induced fluorescence intensity in PNA was equal to ~0.24 mVolt/mTorr. By comparison to this background signal, the LIF signal induced by the dye laser was in the range of 0.18 to 0.22 mV/mTorr (see Table 3 and Figure 6). No laser-induced background appears in the calibration runs with pure H_2O_2.

H_2O_2 impurities in PNA were trapped at -15°C. As a result, the partial pressure of H_2O_2 in the cell was always less than 1 mTorr during PNA runs, as we determined from the intensity of the mass peak at m/e = 34. Thus, the correction to the OH quantum yield from PNA due to photodissociation of H_2O_2 impurity is calculated to be less than 5%.

The PNA quantum yield measurements were conducted when the concentration of HNO_3 impurity was less than 10%. The photodissociation of HNO_3 at 248 nm produces OH radicals with a quantum yield of 1.[10] The absorption cross section of HNO_3 at this wavelength is 20 times lower than that of PNA. As a

result, the correction to our measured OH quantum yield due to photodissociation of HNO_3 impurity is less than 3%. The value of $\Phi = 0.29 \pm 0.13$ suggests sizeable but not predominant OH photoproduct from PNA excitation. The quoted error bars are two standard deviations added in quadrature from the deviations in the averaged intensities of Figure 8.

C. Determination of the PNA Purity Level

The most difficult part of this study was associated with characterizing the purity and amounts of PNA in the reactor during a given experiment. This section details some of the precautions taken and illustrates the difficulty in obtaining precise values for quantum yields. In the course of this study, we investigated over 60 PNA batches. The observations led us to a characterization of the purity of the PNA sample present in the reactor according to the following three criteria:

(1) The first criterion is the magnitude of the ratio of the mass spectrometric signal from mass 30 to mass 46 in the PNA spectrum. This ratio was constantly monitored during a run. As described in the Experimental section, mass 30 and 46 (NO^+ and NO_2^+) are common peaks to PNA, HNO_3, and NO_2. The respective sensitivities are given in Table 1. The ratio 30/46 in NO_2 is ~6, while this ratio is ~0.7 in a typical PNA run.

During runs where wall decomposition was important, i.e., NO_2 and O_2 were formed from PNA, the ratio 30/46 was dramatically enhanced due to both a decrease in mass 46 and an increase in mass 30. This behavior could be reversed by pumping the decomposition products through the vacuum line and then flowing fresh PNA vapor into the reactor. The ratio 30/46 was also larger (2.0 to 4.0) when PNA was first flowed into the cell at the beginning

of a run, and decreased to the 0.7 value within ~15 min. This time represents the expected period necessary to treat the reactor walls, and has been observed in previous work on PNA.[5] When wall decomposition was important, a larger enhancement of the signal of mass 32 is also observed, concurrent with the increase in the ratio 30/46. This peak (O_2^+) is common to the mass spectra of PNA H_2O_2 and O_2 but is much more sensitive to oxygen than to the other compounds. A large intensity at mass 32 in therefore another sign that the decomposition of PNA on the wall is large. LIF measurements were not conducted when the peak at mass 32 was larger than the peak at mass 30 (see Table 1). These two scenarios for large wall decomposition ("dirty" walls or active reactor walls during "treating" period) clearly suggest that a low steady value of 0.7 for the ratio 30/46 indicates a near absence of wall decomposition and a relatively clean batch synthesis. As a result, the amount of NO_2 impurity in batches we consider good (characterized by a 30/46 mass ratio at ~0.7) is believed to be smaller than 5%.[5]

A similar analysis of the HNO_3 mass spectral sensitivity at mass 30 and 46 is possible but less conclusive. The reason is that the HNO_3 intensities are much smaller than those due to PNA, both at mass 30 and 46, and therefore a variation in the amount of HNO_3 impurity from one PNA batch to the other will produce less dramatic changes in the mass spectrum. The yield of HNO_3 impurity in a PNA batch is enhanced if the H_2O_2 sample used is concentrated less than 90% or if the NO_2BF_4 sample is contaminated by water during the PNA synthesis.[21] When this was the case, we observed a larger value of the 30/46 ratio, 1.2 to 1.6, during the corresponding run. (The value of the ratio is ~1.3 for pure HNO_3.) We related this higher value of the ratio 30/46 to a higher concentration of HNO_3 impurity and did not conduct quantum yield

measurements under such conditions. We believe that most of the PNA batches carefully synthesized with pure samples of H_2O_2 and NO_2BF_4, which give rise to the typical PNA mass spectrum shown in Figure 2, contain less than 10% HNO_3 impurity.[5] The intensity of the parent peak of HNO_3 (m/e = 63) did not provide a measurement of the HNO_3 concentration because it is also a small peak in the pure PNA mass spectrum.

Another experiment was undertaken to assess whether or not most of the signal intensity at mass 30 and 40 could be assigned to PNA during good runs. We monitored the changes at mass 30 and 46 during photodissociation at an excimer laser repetition rate of 40 Hz. At this repetition rate and at a laser fluence of 20 mJ/cm^2/pulse, the photolysis rate during the residence time of PNA in the reactor is 7% for PNA. The photolysis rates of HNO_3 ad NO_2 are 0.5 and 0.6% respectively under these conditions and therefore negligible with respect to changes in the mass spectrum. In these experiments we could then expect a 7% decrease at mass 30 and 46. We actually observed a decrease of only ~4% at mass 46 and an increase of ~1% at mass 30 during good runs (ratio 30/46 = 0.7). This measurement indicates that the mass spectrometric intensity of the sum of the photodissociation products from PNA is of the order of 27 mV/mTorr at mass 30 and 14 mV/mTorr at mass 46. These values show that NO_2 cannot be the only such photoproduct but could be accompanied by NO_3 for example. The mass spectrum of NO_3 is not known at mass 30 and 46,[7] but probably has an electron impact cracking pattern at mass 30 and 46 similar to HNO_3. It is also not known if the NO_3 radical will survive until reaching the ion source (~4 s).

(2) The second criterion used to define a pure batch of PNA was the absolute intensity of mass 33. Mass 33 (HO_2^+) is the only peak characteristic

solely of PNA. Pure H_2O_2 also has a small mass peak at mass 33 but was trapped during PNA runs. During good runs as defined above, the sensitivity at mass 33 is 3 mV/mTorr and the intensity at mass 33 is ~12% of that at mass 30. During "bad" runs, the intensity of mass 33 falls to levels as low as ~4% of that of mass 30. A high intensity at mass 33 was always found to be correlated with a value of the ratio 30/46 near 0.7 and with values of the absolute intensity at mass 30 and 46 stated in Table 3.

(3) The third criterion used to define a good run is that the excimer-laser-induced emission detected by the filtered phototube used for the LIF measurements is steady and proportional to the pressure in the cell. Again, this correlates with criteria (1) and (2). Important wall decomposition or less pure PNA batches lead to an excimer-induced emission from PNA of reduced intensity.

In summary, LIF measurements reported above were performed only when the PNA sample flowing in the VLPΦ cell was observed to be as pure as possible, given the impurities inherent in the PNA synthesis (<5% of NO_2 and < 10% of HNO_3).[5] These good conditions are defined by a mass spectrum which presents a small ratio NO^+/NO_2^+ (~0.7), an O_2^+ peak smaller than the NO^+ peak, and a high (3 mV/mTorr) intensity of the HO_2^+ peak. As a result of this estimated impurity level, a 15 ± 5% correction must be made to the PNA partial pressures of Figure 7 and 8 in calculating Φ.

IV DISCUSSION

The nature of the electronically excited states of pernitric acid, in the ultra-violet has been discussed in a recent theoretical study

made by Saxon and Liu.[6] These calculations predict the two lowest excited states of PNA at 5.2 and 6 eV above the ground state in the vicinity of our excitation energy at 248 nm (5 eV). At this wavelength (40322 cm^{-1}) the energy is sufficient to access the following photoproducts of pernitric acid:[6]

(1) $HO_2 + NO_2$ + 92 kcal/mole

(2) $HO_2 + NO_2^*$ (1^2B_2 or 1^2B_1) + 20 or 64 kcal/mole

(3) $HO_2 + NO + O$ + 20 kcal/mole

(4) $OH + NO_3$ + 75 kcal/mole

(5) $OH + NO_2 + O$ + 26 kcal/mole

The theoretical study of Saxon and Liu suggests that channels forming OH + NO + O_2, HNO + O_3, HNO_2 + O_2, and HNO_3 + O are unlikely because they require extensive rearrangement. Therefore, we will focus the discussion on the channels which form HO_2 + NO_2 and the ones that form OH + NO_3. An energy diagram of these photolysis products of HO_2NO_2 is given in Figure 9. The bond energy values and the energies of the two first excited states of NO_2 used in this figure are taken from the literature.[6,12] The lefthand side of the figure shows the energy threshold for each photodissociation pathway of HO_2NO_2 producing OH. The ground state of HO_2NO_2 is taken as the origin of energy. The energy threshold for ground state OH + NO_3, is 14000 cm^{-1}, the threshold for ground state OH + NO + O_2 is 15250 cm^{-1}, and the threshold energy for

ground state OH + NO_2 + O is 31241 cm^{-1}. The right hand side of Figure 9 shows the photodissociation pathways of HO_2NO_2 leading to an HO_2 radical. The energy thresholds for HO_2 + NO_2 (X^2A_1), $NO_2(1^2B_2)$, and $NO_2(1^2B_1)$ are 8065, 17865, and 22813 cm^{-1} respectively. The energy threshold for ground state OH + NO + O is 33280 cm^{-1}.

In the experimental work described in the previous section we showed evidence for the formation of electronically excited NO_2 and ground state OH produced by single photon absorption of PNA. We also observed a weak channel forming $OH(A^2\Sigma^+)$ following three photon absorption by PNA. We discuss successively our results concerning the NO_2^* channel and the OH ground state channel.

A. Fluorescence emission from NO_2^*

Our observations of the NO_2^* emission produced upon photolysis of HO_2NO_2 at 248 nm are similar to those of Oh, et. al.,[12] on the NO_2^* emission produced upon photolysis of N_2O_5 at 266 nm. This work was published during the course of this study, and our intepretation is similar to theirs.

In Figure 9 (righthand side, shaded area) we have drawn schematically the experimental energy distribution of the fluorescence emission from PNA, relative to the energy of the NO_2 ground state. In Figure 9 we used the spectrum recorded with the R666 photomultiplier tube (Figure 4) which has a flat response over most of the fluorescence emission spectrum. This energy distribution is related to but does not reflect exactly the population distribution of the two first excited states of NO_2 ($1\ ^2B_2$) and ($1\ ^2B_1$) because we observe emission not only from these states to NO_2 ($X^2A_1, v = 0$) but also from these states to NO_2 ($X^2A_1, v > 0$). The excess energy available after

breaking the weak HO_2NO_2 bond (8065 cm^{-1}) is 32260 cm^{-1}. This energy is partitioned between the vibrational, rotational, and translational energy of the HO_2 and the NO_2 fragments:

$$HO_2NO_2 + h\upsilon(248\ nm) \rightarrow HO_2(V,J) + NO_2^*(V,J) + E(translation)$$

If the sum of the electronic, vibrational and rotational internal energy stored in the NO_2 does not exceed the energy of the N-O bond (25215 cm^{-1}), NO_2 will be formed with vibrational and rotational excess energy in either the ground state or one of the two first excited states ($^2B_2$ and $^2B_1$). The energy threshold for breaking the N-O bond in NO_2 is 33280 cm^{-1} (see Figure 9), which corresponds to a short wavelength emission threshold of 397 nm. Actually, all of our experimental spectra show a threshold ≥ 400 nm. We observed that the experimental threshold depends slightly on the time of observation of the fluorescence. The spectra from PNA shown in Figure 5 were taken at a delay time of 500 ns after the photolysis laser pulse and show a threshold of ~420 nm. The spectrum from PNA shown in Figure 4 was taken at a delay time of 50 ns and shows a threshold of ~400 nm. The fact that the lower wavelength threshold shifts towards the red when the delay time increases is likely to be associated with vibrational relaxation of NO_2^* states having an energy just below the NO-O dissociation limit.

The maximum of the emission at 558 nm suggests that the maximum population is in $NO_2(1^2B_2)$ with 8140 cm^{-1} vibrational energy or in $NO_2(1^2B_1)$ with 3190 cm^{-1} vibrational energy (see Figure 9.). There is also a smaller maximum or shoulder in the fluorescence spectrum at 460 nm (see Figure 4 and 5). This value would correspond to a vibrational energy of 6990 cm^{-1} and

11940 cm^{-1} for NO_2 in the (1^2B_2) and (1^2B_1) excited state, respectively.

In parallel to the above discussion of PNA, we can consider the energy balance in the photodissociation of HNO_3 for which we observed a similar fluorescence emission (see Figure 4). The energy of the bond $HO-NO_2$ is 16,672 cm^{-1}.[22] At 248 nm (40322 cm^{-1}), the excess energy available after breaking this bond is 23650 cm^{-1}. This energy is lower than the excess energy available in PNA after breaking the HO_2NO_2 bond, 33280 cm^{-1}. This fact is consistent with the red shift experimentally observed in the NO_2^* emission from HNO_3 versus that from PNA. Furthermore, in the HNO_3 case, this excess energy is not sufficient to break the N-O bond in NO_2, which is in agreement with the known quantum yield of unity for the formation of NO_2 from photodissociation of HNO_3 at 248 nm.[10] It is also known (as noted earlier)[18] that OH is formed vibrationally and rotationally cold in the photodissociation of HNO_3. Therefore all the excess energy (except for translation) is available to produce NO_2 electronically excited, and one may speculate a large quantum yield for production of NO_2^* from HNO_3. By assuming $\Phi = 1$, we can calculate an upper limit for the quantum yield of NO_2^* from PNA, by comparing the fluorescence intensity of the two emissions integrated over the wavelength range 300-800 nm (see Figure 5). The ratio of the integrated NO_2^* fluorescence intensity from PNA versus that from HNO_3 is ~6. (The ratio of 5 given in Table 2 is the ratio of the relative intensities at the maximum of the PNA fluorescence emission, 558 nm). The ratio of the absorption cross section of PNA versus HNO_3 at 248 nm is 20. As a result an upper limit of the quantum yield for production of NO_2^* from photodissociation of PNA at 248 nm is 6/20, that is ~30%. The actual value for Φ is almost certainly somewhat lower than 0.3, because it is unlikely that the NO_2 photoproduct from HNO_3 is

produced only in electronically excited states. A large density of vibrational levels is available in the ground state to accomodate the excess energy, and it is known that some is also channeled into translation. We also note, however, that N_2O_5 photolysis at 266 nm [12] gives a 25% quantum yield for NO_2^* emission.

We finally apply a similar interpretation of the energy partitioning in the photoexcitation of NO_2 at 248 nm (40322cm^{-1}). The transition corresponds to excitation of the 2^2B_2 state of NO_2 which lies at 40140 cm^{-1} above NO_2 ground state. Tsukiyama, et. al.,[23] have observed an emission from $NO_2(2^2B_2)$ to $NO_2(1^2B_2)$ upon photoexcitation of NO_2 at 249 nm and measured a lifetime of the $NO_2(2^2B_2)$ state shorter than 7 ns. The NO_2 molecules on the (1^2B_2) state can then emit to the ground state in the visible. This is a process consistent with our experimental observation of an emission from $NO_2(1^2B_1)$ or (1^2B_2) state to NO_2 ground state upon photoexcitation at 248 nm (see Figure 4). However, this process is likely to be a minor pathway and also strongly wavelength-dependent because the 248 nm radiation brings NO_2 to an energy level which is 15100 cm^{-1} above the dissociation limit to the channel NO + O. The quantum yield for NO production from photodissociation of NO_2 has not been measured at 248 nm, but has been estimated to be 0.98 at 295 nm from extrapolation of measurements between 375 and 420 nm.[10] Our experimental observation of an NO_2^* emission demonstrates that the NO quantum yield is smaller than (but possibly close to) unity from photodissociation of NO_2 at 248 nm. If an absolute measurement of the NO_2^* quantum yield from photoexcitation of either NO_2 or HNO_3 at 248 nm becomes available we will be able to calculate the absolute quantum yield for NO_2^* from PNA, by comparing the observed NO_2^* fluorescence intensities given in Table 2.

B. Measurement of the OH Quantum Yield.

We have measured a quantum yield (Φ) for production of OH radicals from the photodissociation of HO_2NO_2 at 248 nm. The measured value of Φ is 0.29 + 0.13 (see Table 3 and Figure 8). This value was obtained from the LIF measurements on the $Q_1 5$ OH line. The measurements we conducted on the $Q_1 1,1'$ line, in order to confirm the value of Φ, show an unexpected increase of the pressure normalized LIF intensity with increasing H_2O_2 pressure, from 0.2 at 5 mTorr to 0.6 at 17 mTorr (see Figure 7 and Table 3). The $Q_1 1,1'$ data for PNA do not show such a pressure dependence. A likely explanation derives from the fact that the OH is produced rotationally hotter from H_2O_2 photodissociation than from PNA. Since relaxation to a thermal population of N = 1 requires more collisions, the pressure dependence is observed for this level but not for N = 5. This agrees with our observation of the OH rotational temperature measurements that the thermalization of OH from H_2O_2 is not complete at a delay time of 3μs. (At longer delays it is difficult to monitor the OH concentrtation from PNA.) In contrast, the fractional population of N = 5 in a Boltzmann distribution is constant to within 12% over the 500-1200K temperature range. As a result, the calibration against the LIF intensity of the $Q_1 5$ line allows a statistically significant analysis of the OH concentration, even if full equilibrium has not been achieved.

The uncertainty in the quantum yield due to the possible contribution to OH formation from photodissociation of H_2O_2 or HNO_3 impurities has been shown to be negligible compared to the uncertainty in the quantum yield measurement itself. The contribution to OH formation from absorption of a second 248 nm photon by the photofragment HO_2 ($\sigma_{HO_2} = 5 \times 10^{-19}$ cm^2 a 248 nm) amounts to at

most 10^{-3} of the OH quantum yield. Finally, the measured value of the OH quantum yield of ~30% is a lower limit considering that the PNA sample in the VLPΦ cell is not pure. On the basis of a realistic 15 ± 5% impurity level of the PNA sample, the corrected quantum yield is 34 ± 16%.

The fluorescence emission spectra from PNA (see Figure 3) show a small channel producing OH ($A^2\Sigma^+$) in a 3-photon absorption process. On energetic grounds, we know that at least two photons are required to access this state from PNA at 248 nm. While the exact mechanisms that lead to the formation of OH^* from PNA (and HNO_3) are not known, we can state from the observed intensities of the LIF signal that the 3-photon process constitutes only a minor pathway compared to the OH ground state formed in a 1-photon process.

V CONCLUSION

The photodissociation of pernitric acid, HO_2NO_2, was studied at 248 nm. Two photodissociation pathways were identified, OH + NO_3 and HO_2 + NO_2^*. The quantum yield for production of OH radicals was measured to be 34 ± 16%. NO_2 was found to be produced in its electronic excited states (1^2B_2 and/or 1^2B_1). We determined an upper limit of the quantum yield for production of NO_2^* of 30%. We can only speculate as to the nature of the remaining photodissociation pathway(s). Given the observation that formation of NO_2^* is an important pathway and given the excess energy available, it is likely that the HO_2 + NO + O channel is also populated. A major channel producing ground state NO_2 + HO_2 also seems likely. Assuming that the quantum yields are not very different at 290 nm, atmospheric models using

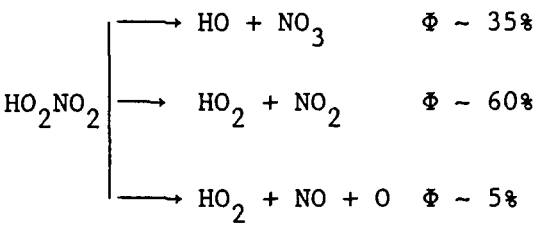

will be adequate for most purposes. These photoproducts are largely interconnectable by subsequent chemistry.

ACKNOWLEDGMENTS

It is a pleasure to thank H. Helm for helpful discussions during the course of this experiment. This work was supported by NASA under contract No. NASW-3888.

REFERENCES

1. Atmosphere Ozone 1985, WMO Report #16, pp. 33-34.

2. P. L. Trevor, G. Black, and J. R. Barker, J. Phys. Chem. 86, 1661 (1982).

3. I. Barnes, V. Bastian, K. H. Becker, E. H. Fink, and F. Zabel, Atmospheric Environment 16, 545 (1982).

4. C. A. Smith, L. T. Molina, J. J. Lamb, and M. J. Molina, Int. J. Chem. Kinet. 16, 41 (1984).

5. L. T. Molina and M. J. Molina, J. Photochem 15, 97 (1981), and references therein.

6. R. P. Saxon and B. Liu, J. Phys. Chem. 89, 1227 (1985).

7. (a) J. S. Chang, J. R. Barker, J. E. Davenport, and D. M. Golden, Chem. Phys. Lett. 60, 3851 (1979); (b) J.R. Barker, L. Brouwer, R. Patrick, M.J. Rossi, P.L. Trevor, and D.M. Golden, Int. J. Chem. Kinetics 17, 991 (1985).

8. R. A. Kenley, P. L. Trevor, and B. Y. Lan, J. Am. Chem. Soc. 103, 2203 (1981).

9. C. B. McKendrick, E. A. Kerr, and J.P.T. Wilkinson, J. Phys. Chem. 88, 3930 (1984).

10. W. B. DeMore, J. J. Margitan, M. J. Molina, R. T. Watson, D. M. Golden, R. F. Hampson, M. J. Kurylo, C. J. Howard, A. R. Ravishankara, in Chemical Kinetics and Photochemical Data for Use in Stratospheric Modeling, Evaluation Number 7, JPL Publication 85-37 (1985).

11. A. Fontijn, C. B. Meyer, and H. I. Schiff, J. Chem. Phys., 40, 64 (1964).

12. D. Oh, W. Sisk, A. Young, and H. Johnston, J. Chem. Phys., 85, 7146 (1986).

13. V. M. Donnelly, D. G. Keil, and F. Kaufman, J. Chem. Phys. 71, 659 (1979), and references therein.

14. K. R. German, J. Chem. Phys. 62, 2584 (1975).

15. R. Bersohn and M. Shapiro, J. Chem. Phys., 85, 1396 (1986).

16. K.-H. Gerike, S. Klee, and F. J. Comes, J. Chem. Phys., 85, 4463 (1986).

17. V. Vasudev, R. N. Zare, and R. N. Dixon, J. Chem. Phys. 80, 4863 (1984).

18. A. Jacobs, K. Kleinermanns, H. Kuge, and J. Wolfrum, J. Chem. Phys., 79, 3162 (1983).

19. I. L. Chidsey and D. R. Crosley, J. Quant. Spect. Rad. Transfer, 22, 187 (1980).

20. G. Ondrey, N. van Veen, and R. Bersohn, J. Chem. Phys., 78, 3732 (1983).

21. L.T. Molina and M.J. Molina, private communication.

22. JANAF Thermochemical Tables, Second ed., NSRDS-NBS 37, 1971.

23. K. Tsukiyama, K. Shibuya, K. Obi, and I. Tanaka, J. Chem. Phys., 82, 1147 (1985).

Table 1

MASS SPECTRAL INTENSITIES

in mV/mTorr, FOR PNA, HNO_3, NO_2, AND H_2O_2

m/e	30	32	33	34	46	63	85
Ion	NO^+	O_2^+	HO_2^+	$H_2O_2^+$	NO_2^+	HNO_3^+	SiF_3^+
PNA	24	20	3		33	.02-.1	.1-.4
HNO_3	14				11	~.05	
NO_2	40				7		
H_2O_2	3	2	20				

Table 2

RELATIVE INTENSITY OF THE FLUORESCENCE EMISSION
FROM PHOTOEXCITATION OF PNA, HNO_3, AND NO_2 AT 248 nm

	Fluorescence Relative Intensity at 558 nm (arbitrary units)	Absorption Cross Section at 248 nm (cm^2)
PNA	42	42×10^{-20}
HNO_3	8	2×10^{-20}
NO_2	2.2	3×10^{-20}

Table 3

QUANTUM YIELD Φ FOR PRODUCTION OF OH RADICALS
FROM PNA PHOTODISSOCIATION

	$\Psi_{H_2O_2}$(a)	$I_{H_2O_2}$(b) (mV/mTorr)	Ψ_{PNA}	I_{PNA} (mV/mTorr)	Φ
	0.002		0.01		
$Q_1 1,1'$		0.2 to 0.6 (c)		0.22 ± 0.12	
$Q_1 5$		0.25 ± 0.04		0.18 ± 0.08	0.29 ± 0.13 (d)
					0.34 ± 0.16 (e)

(a) photodissociation rates per pulse

(b) normalized LIF signal.

(c) pressure dependent

(d) assuming that the total pressure is that of pure PNA

(e) corrected for PNA partial pressure

Figure 1 Schematic view of the very low pressure photolysis (VLPΦ) apparatus. The reactant gas flows into the cell from the preparation line and is analysed by a modulated molecular beam quadrupole mass spectrometer. The reactant is photodissociated by the excimer laser which fills the center of the cell (shaded area). OH radicals are detected by laser induced fluorescence (LIF) using a tunable excimer-pumped-dye laser. Alternatively, a monochromator with proper collection lenses is set in front of the LIF window to detect the excimer-induced-fluorescence of the reactant gas.

Figure 2 Mass spectrum of a typical PNA sample flowing from the cell detected by the molecular beam quadrupole mass spectrometer. The resolution is one mass unit at mass 63.

Figure 3 Fluorescence emission spectrum following PNA photodissociation at 248 nm. The PNA spectrum was recorded with the R666 PMT, at low resolution (~5 nm), at a delay time of 50 ns following the excimer pulse, with a 1 μs observation gate. The insert shows a portion of the spectrum in the vicinity of the OH(A-X) (0,0) band obtained at higher resolution (~2 nm). The pressure in the cell was ~150 mTorr. The two dotted curves represent the spectra obtained by Oh et al.[12] in the photolysis of N_2O_5 at 266 and 304 nm.

Figure 4 Comparison of fluorescence emission spectra obtained for PNA, NO_2 and HNO_3 after irradiation at 248 nm. The three spectra were recorded with the 1P28 PMT, at low resolution (~5 nm), at a delay time of 500 ns after the laser pulse, with a 1 μs observation gate. The pressure was ~150 mTorr for each of the three gases.

Figure 5 Decay rates of the NO_2^* emission at 558 nm, following PNA photodissociation at 248 nm. The decay rates were obtained from exponential fits to the measured fluorescence decay, and are shown as a function of pressure. The squares are data obtained in pure PNA. The triangles are data obtained in a mixture of PNA with argon. The lines drawn represent least squares fits of the data.

Figure 6 Laser-induced-fluorescence (LIF) excitation spectrum of the OH(A-X) (1,0) band obtained from H_2O_2 (lower trace) and from PNA (upper trace). The delay time was 5 μs between the photolysis pulse and the probe pulse. The pressure was ~20 mTorr in both cases. The intensity of the OH LIF spectrum from PNA is amplified 2.5 times more than that from H_2O_2. The hatched area represents the excimer laser induced fluorescence background from PNA transmitted through the 313 nm filter.

Figure 7 Pressure normalized intensities of the OH LIF signal obtained from PNA (squares) and from H_2O_2 (triangles) following for $Q_1$1,1' line excitation, as a function of pressure. The line represents the average over the PNA data. The OH LIF normalized intensities from H_2O_2 show a pressure dependence indicating rotational relaxation (see Discussion).

Figure 8 Pressure normalized intensities of the OH LIF signal obtained from PNA (squares) and from H_2O_2 (triangles) following $Q_1$5 line excitation, as a function of pressure. The intensities measured in H_2O_2 have been multiplied by 2 for clarity. The two lines represent the average over the PNA data and the H_2O_2 data respectively.

Figure 9 Energy diagram for HO_2NO_2 and some of its photodissociation product channels at 248 nm. The hatched area indicates the energy distribution of the experimental NO_2 fluorescence emission observed upon photodissociation of HO_2NO_2 at 248 nm.

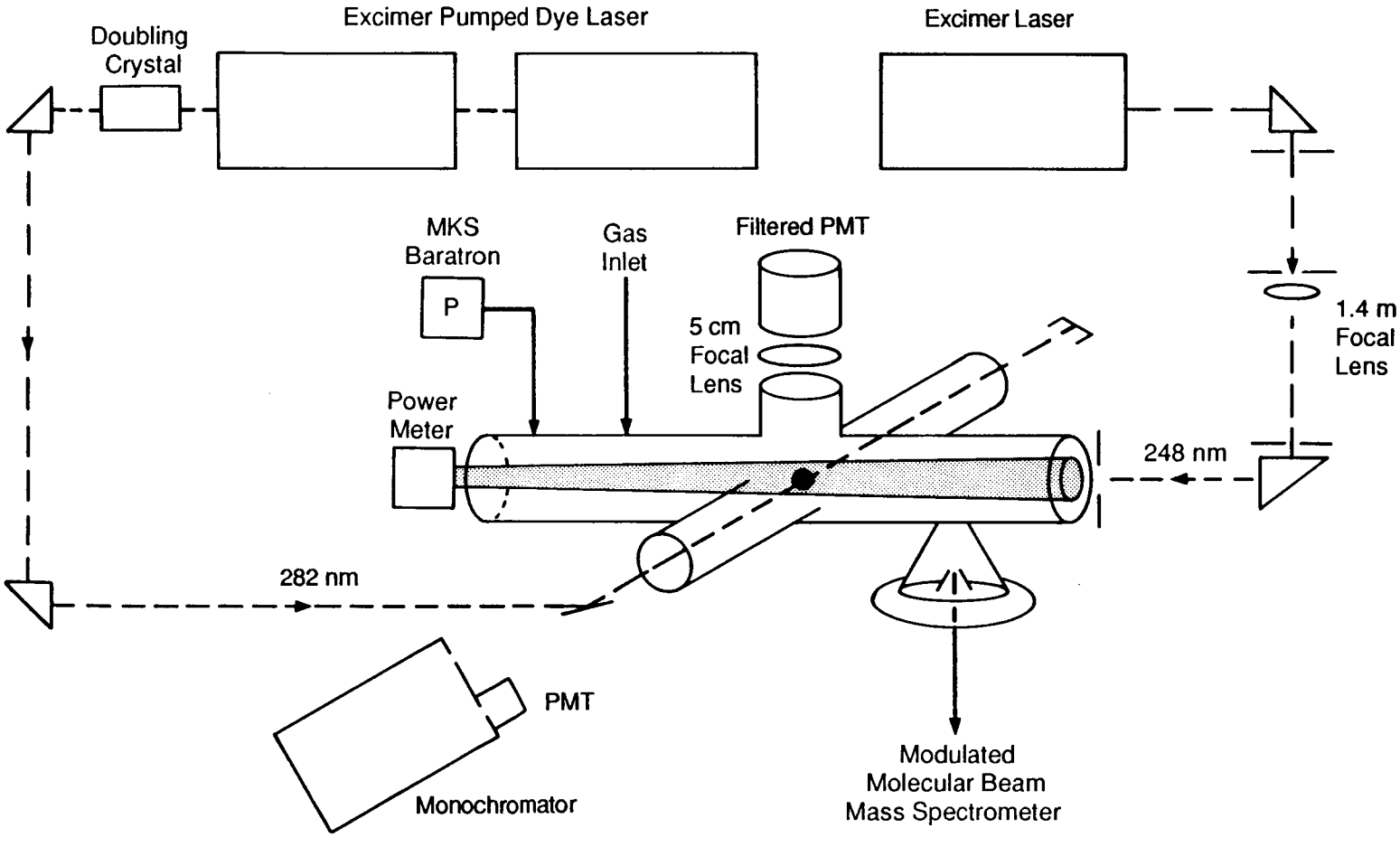
Doubling Crystal
Excimer Pumped Dye Laser
Excimer Laser
MKS Baratron
P
Gas Inlet
Filtered PMT
5 cm Focal Lens
1.4 m Focal Lens
Power Meter
248 nm
282 nm
PMT
Monochromator
Modulated Molecular Beam Mass Spectrometer

JA-m-7140-5A

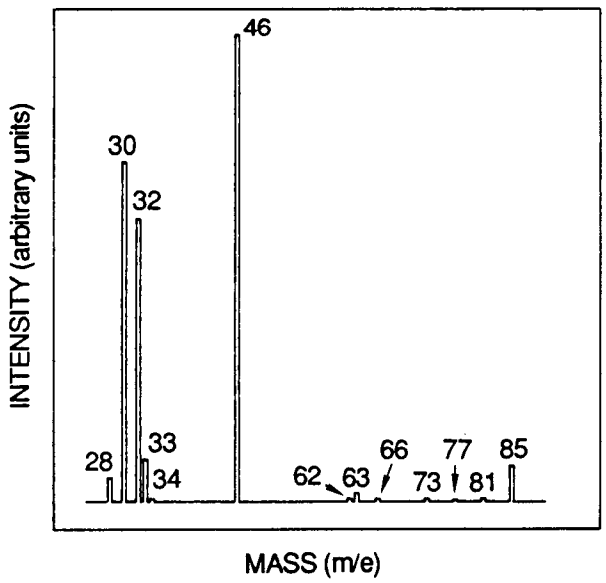
INTENSITY (arbitrary units)
46
30
32
28
33
34
62
63
66
73
77
81
85
MASS (m/e)

JA-m-7140-14

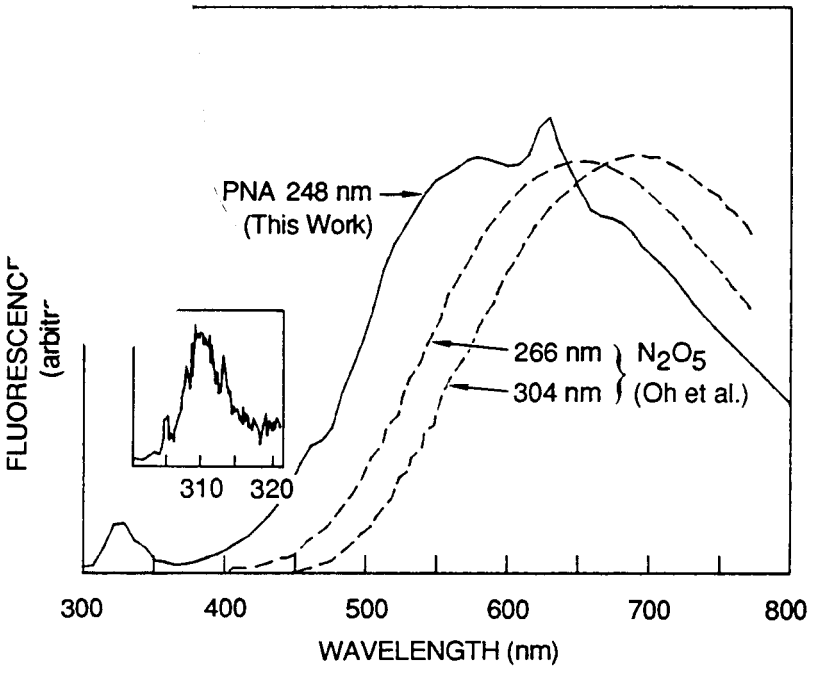
PNA 248 nm
(This Work)
266 nm
304 nm
N_2O_5
(Oh et al.)
310
320
FLUORESCENCE
(arbitr
300
400
500
600
700
800
WAVELENGTH (nm)

JA-m-7140-18

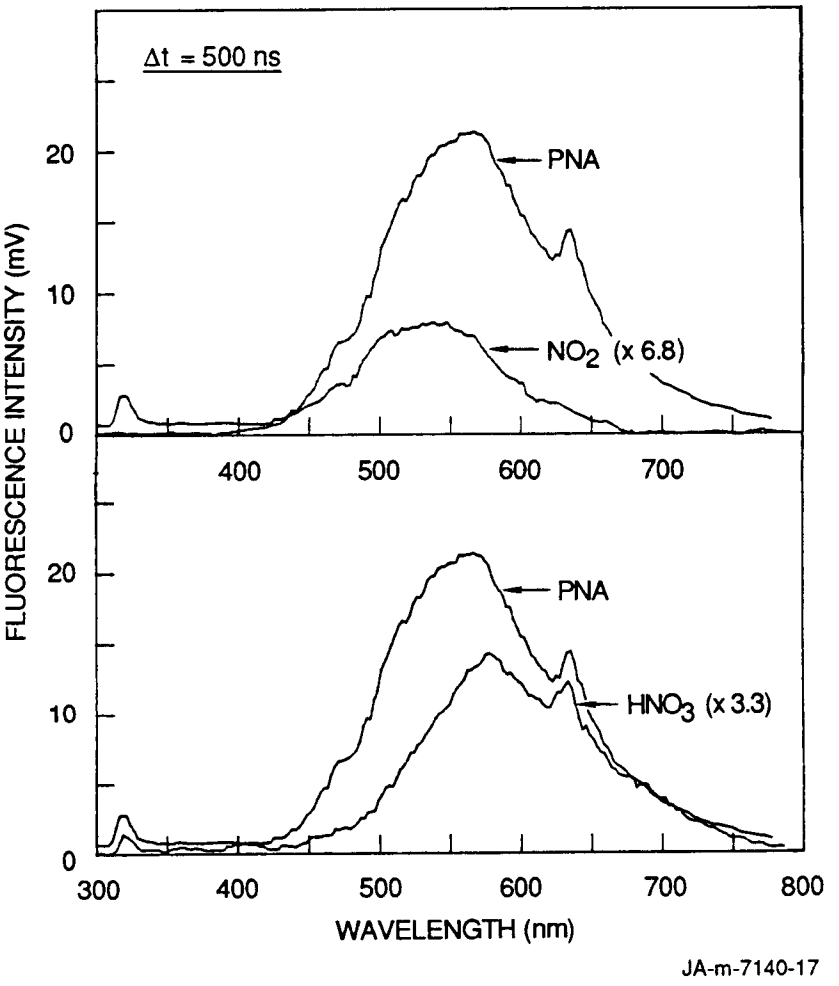
Δt = 500 ns
PNA
NO2 (x 6.8)
PNA
HNO3 (x 3.3)
FLUORESCENCE INTENSITY (mV)
WAVELENGTH (nm)
0
10
20
300
400
500
600
700
800

JA-m-7140-17

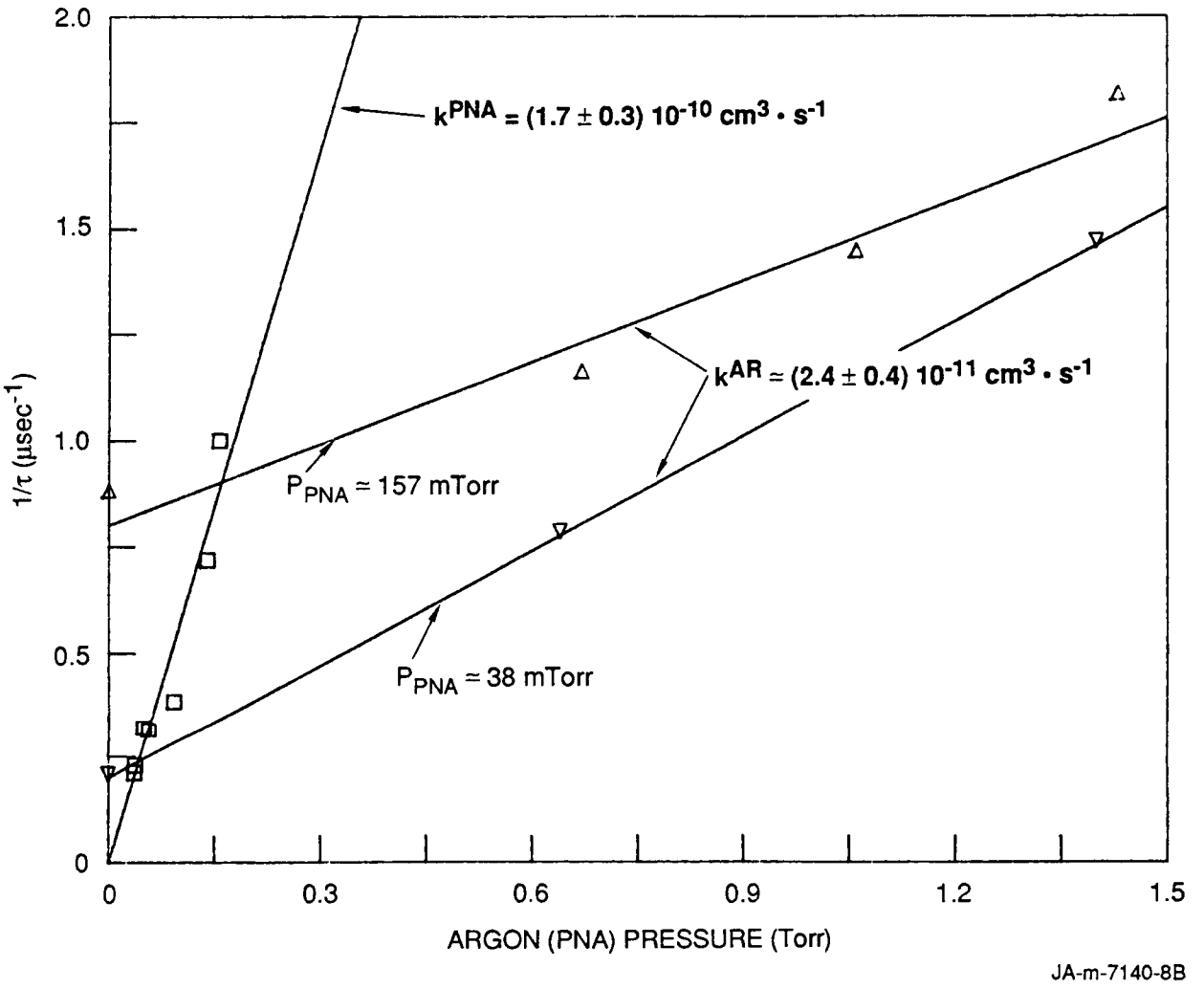
2.0
1.5
1.0
0.5
0
1/τ (μsec⁻¹)
k^PNA = (1.7 ± 0.3) 10⁻¹⁰ cm³ • s⁻¹
k^AR = (2.4 ± 0.4) 10⁻¹¹ cm³ • s⁻¹
P_PNA = 157 mTorr
P_PNA = 38 mTorr
0
0.3
0.6
0.9
1.2
1.5
ARGON (PNA) PRESSURE (Torr)

JA-m-7140-8B

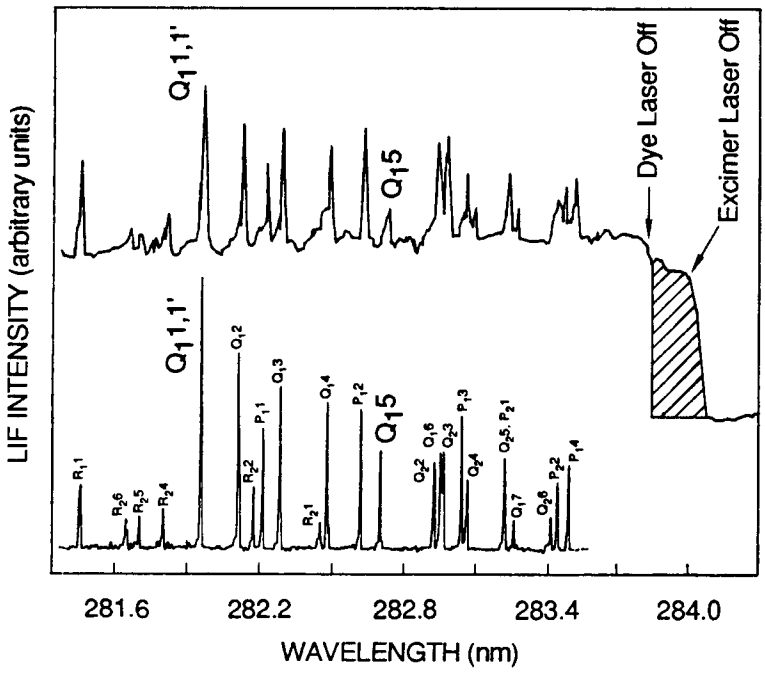
LIF INTENSITY (arbitrary units)
Q1 1,1'
Q15
Dye Laser Off
Excimer Laser Off
R1,1
R2,6
R2,5
R2,4
Q1 1,1'
Q1,2
R2,2
P1,1
Q1,3
R2,1
Q1,4
P1,2
Q15
Q2,2
Q1,6
Q2,3
P1,3
Q2,4
Q2,5, P2,1
Q1,7
Q2,6
P2,2
P1,4
281.6
282.2
282.8
283.4
284.0
WAVELENGTH (nm)

JA-m-7140-19

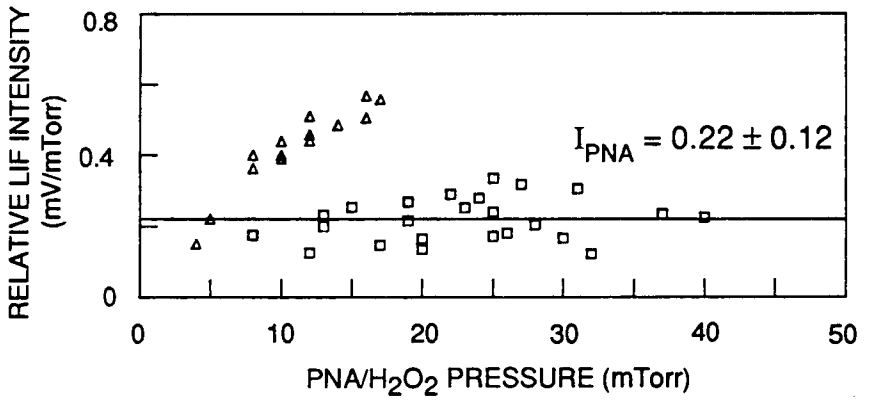
RELATIVE LIF INTENSITY
(mV/mTorr)
0.8
0.4
0
0
10
20
30
40
50
$I_{PNA} = 0.22 \pm 0.12$
PNA/H_2O_2 PRESSURE (mTorr)

JA-m-7140-15

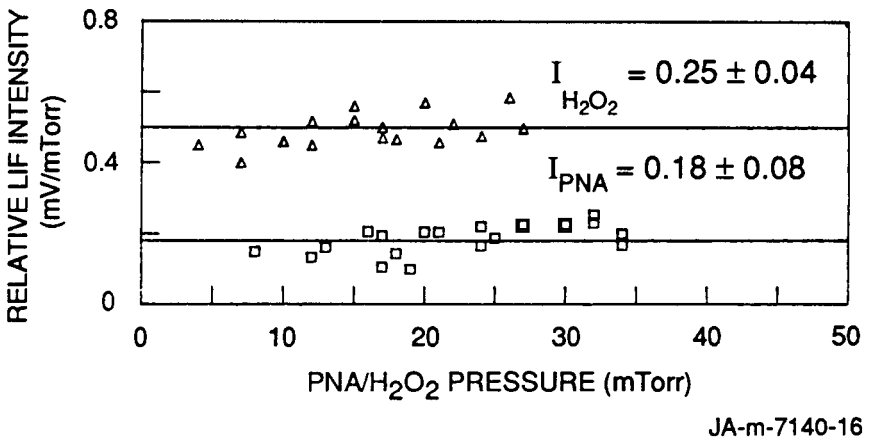
RELATIVE LIF INTENSITY
(mV/mTorr)
0.8
0.4
0
0
10
20
30
40
50
$I_{H_2O_2} = 0.25 \pm 0.04$
$I_{PNA} = 0.18 \pm 0.08$
PNA/H_2O_2 PRESSURE (mTorr)

JA-m-7140-16

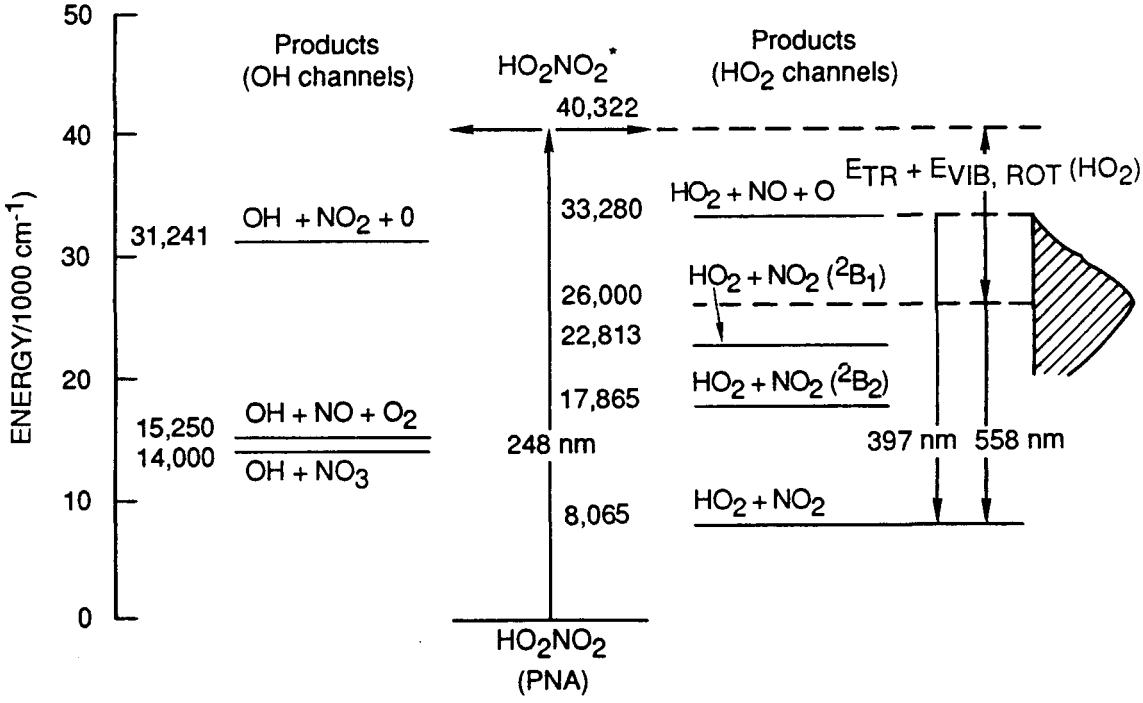
50
40
30
20
10
0
ENERGY/1000 cm-1
Products
(OH channels)
HO2NO2*
40,322
Products
(HO2 channels)
31,241
OH + NO2 + 0
33,280
HO2 + NO + O
ETR + EVIB, ROT (HO2)
26,000
HO2 + NO2 (2B1)
22,813
15,250
14,000
OH + NO + O2
OH + NO3
17,865
HO2 + NO2 (2B2)
248 nm
397 nm
558 nm
8,065
HO2 + NO2
HO2NO2
(PNA)
JA-m-7140-20